

Shadowing unstable orbits of the Sitnikov elliptic 3-body problem

D. J. Urminsky*

*Department of Physics and Centre for Computational Relativity and Gravitation, Rochester Institute of Technology,
85 Lomb Memorial Drive, Rochester, NY, 14623, USA*

10 May 2010

ABSTRACT

Errors in numerical simulations of gravitating systems can be magnified exponentially over short periods of time. Numerical shadowing provides a way of demonstrating that the dynamics represented by numerical simulations are representative of true dynamics. Using the Sitnikov Problem as an example, it is demonstrated that unstable orbits of the 3-body problem can be shadowed for long periods of time. In addition, it is shown that the stretching of phase space near escape and capture regions is a cause for the failure of the shadowing refinement procedure.

Key words: celestial mechanics, stellar dynamics, methods: numerical

1 INTRODUCTION

The sensitivity which N -body integrations exhibit to small changes in initial conditions and to numerical errors has been an active area of research since Miller’s landmark study. Miller (1964) demonstrated the exponential divergence of near-by orbits for systems with $N \leq 32$ and found that the separation of nearby orbits increases rapidly when close binary interactions occur. He suggested that the divergence of near-by orbits is too rapid to be solely accounted by binary interactions and suggests that there must be a collective effect to account for the results. However, Standish (1968) showed that the divergence rate was reduced if the potential was replaced with a softened potential and concluded that the divergence is mainly due to close binary interactions.

The dramatic effects of numerical errors on N -body integrations was also demonstrated in an important paper by Lecar (1968). After coordinating a study with 11 different integrations of the same 25-body problem for 2.5 crossing times, Lecar found that quantities such as half mass radius and the moment of inertia can change by as much as 100 percent. In a study with $N = 3$, Dejonghe and Hut (2001) demonstrated that the amplification of initial errors can increase by as much as 10^{20} . In addition, they showed that the growth of errors during close encounters can be amplified by as much as 10^4 , however some of the growth can be recovered after the encounter is over.

The sensitivity to small changes in initial conditions and numerical errors is a property associated with chaotic systems. A measure of the sensitivity of numer-

ical errors can be determined by the Lyapunov exponent λ . Early work suggested that the Lyapunov exponent is inversely proportional to the crossing time t_{cr} (Kandrup and Smith 1991; Heggie 1991; Goodman et al. 1993). However, Goodman et al. (1993) suggest a dependence on N of the form $\lambda^{-1} = t_{cr}/\log N$ or perhaps $\lambda^{-1} = t_{cr}/\log(\log(N))$, implying that as N increases the rate of separation decreases and the Lyapunov exponent increases. The $\log(N)$ dependence was later numerically verified by Hemsendorf and Merritt (1991).

Despite the difficulty calculating solutions to N -body integrations, computers still remain a useful tool to study self gravitating systems. If numerical errors in numerical solutions to the N -body problem cause such drastic changes in the actual positions and velocities of particles how can we trust the dynamics that these solutions represent? Shadowing is a way of proving that a true solution to a dynamical system follows close to a numerical solution. If true orbits can be found close to numerical orbits then the dynamics represented by the numerical solutions represents true dynamics.

This study will discuss the existence of shadow orbits for the gravitational 3-body problem. First, definitions and concepts related to shadowing of dynamical systems will be introduced. Next, a refinement procedure which makes corrections to numerical orbits to reduce the errors incurred at each time step will be presented. The Sitnikov problem will then be presented and used as a simple model to discuss escape and capture of orbits. An approximate Poincaré map is then presented to model orbits of the Sitnikov problem and will be used in conjunction with the refinement procedure to discuss the validity of numerical solutions by way of shadowing. The failure of the refinement procedure to find

* E-mail: urminsky@astro.rit.edu

shadow orbits will then be discussed and regions of phase-space where the procedure fails will be delineated. Finally, it will be demonstrated that the shadow times for this problem can be modeled as a Poisson process.

2 SHADOWING

Consider the autonomous ordinary differential equation

$$\dot{\mathbf{x}} = f(\mathbf{x}), \quad (1)$$

where $\mathbf{x} \in \mathbb{R}^n$ and $f : \mathbb{R}^n \rightarrow \mathbb{R}^n$ is a C^1 vector field with the associated flow represented by ϑ^t . A sequence of points $\{\mathbf{y}_k\}_{k=0}^M$ is said to be a **pseudo-orbit** if there is an associated bounded sequence $\{h_k\}_{k=0}^M$ of positive time such that,

$$|\mathbf{y}_{k+1} - \vartheta^{h_k}(\mathbf{y}_k)| < \delta, \quad (2)$$

for $k = 0, 1, \dots, M$, where $\delta > 0$. An example of a pseudo-orbit is a numerical solution to (1). To show that a pseudo-orbit represents some true dynamics for (1), it would be enough to show that a true orbit follows close to the pseudo-orbit. The pseudo-orbit described above is said to be **shadowed** by a true orbit if there is a sequence of points $\{\mathbf{x}_k\}_{k=0}^M$ and positive times $\{t_k\}_{k=0}^M$ with $\vartheta^{t_k}(\mathbf{x}_k) = \mathbf{x}_{k+1}$ such that

$$|\mathbf{x}_k - \mathbf{y}_k| < \epsilon, \quad (3)$$

and

$$|t_k - h_k| < \epsilon, \quad (4)$$

for $k = 0, 1, \dots, M$ and small $\epsilon > 0$. The sequence $\{\mathbf{x}_k\}_{k=0}^M$ is known as a **shadow-orbit**. The shadow-orbit is a true solution to (1).

The first general contributions made on shadowing for dynamical systems were the shadowing theorems of Anosov (1967) and Bowen (1972). Anosov and Bowen considered hyperbolic systems and showed that any pseudo-orbit on a hyperbolic invariant set has a shadow-orbit. These theorems were generalized for pseudo-orbits in the vicinity of a hyperbolic set (Kato 1991; Nadzieja 1991; Coomes et al. 1995). For non-hyperbolic systems or for orbits which are far from hyperbolic invariant sets these theorems do not apply. Shadowing theorems do exist for pseudo-orbits of non-hyperbolic systems and usually rely on numerical verification of a theorem (Coomes et al. 1994; Chow et al. 1989; Chow and Palmer 1991; Chow and Van Vleck 1994; Van Vleck 1995).

2.1 Refinement procedure

Shadowing N -body simulations was first demonstrated by Quinlan and Tremaine (1992) and Hayes (2001). Both these studies considered the refinement procedure found in Grebogi et al. (1990) to find numerical shadows for the N -body problem. The refinement procedure is a noise reduction technique which can be used to show the existence of shadow-orbits. This procedure will be presented for two dimensional dynamical maps, however the procedure can easily be adapted for flows and has been extended to higher dimensional systems by Quinlan and Tremaine (1992).

Consider the pseudo-orbit $\{\mathbf{p}_k\}_{k=0}^M$ of a map $\mathbf{f} \in \mathbb{R}^2$. The goal is to find a new less noisy orbit $\{\hat{\mathbf{p}}_k\}_{k=0}^M$ close to the original orbit. Let \mathbf{e}_k represent the one step error where

$$\mathbf{e}_k = \mathbf{p}_k - \mathbf{f}(\mathbf{p}_{k-1}). \quad (5)$$

The refined orbit is constructed by

$$\hat{\mathbf{p}}_k = \mathbf{p}_k + \mathbf{\Phi}_k, \quad (6)$$

where $\mathbf{\Phi}_k$ is the correction at time step k . Combine equations (5) and (6) to obtain

$$\mathbf{\Phi}_k = \mathbf{f}(\hat{\mathbf{p}}_{k-1}) - \mathbf{e}_k - \mathbf{f}(\mathbf{p}_{k-1}), \quad (7)$$

where $\hat{\mathbf{p}}_k = \mathbf{f}(\hat{\mathbf{p}}_{k-1})$. Assuming that the correction, $\mathbf{\Phi}_k$, is small, expand $\mathbf{f}(\hat{\mathbf{p}}_{k-1})$ about \mathbf{p}_{k-1} in a Taylor series to get,

$$\mathbf{f}(\hat{\mathbf{p}}_{k-1}) \approx \mathbf{f}(\mathbf{p}_{k-1}) + \mathbf{L}_{k-1}\mathbf{\Phi}_{k-1}, \quad (8)$$

where \mathbf{L}_k is the linearized map at the k th time step. Substitute (8) into (7) to obtain

$$\mathbf{\Phi}_k \approx \mathbf{L}_{k-1}\mathbf{\Phi}_{k-1} - \mathbf{e}_k. \quad (9)$$

It is also assumed that the linearized map has an expanding direction, \mathbf{u}_k , and a contracting direction, \mathbf{s}_k , at each time step k . With this assumption, the objective is to find the sequences $\{\mathbf{\Phi}_k\}_{k=0}^M$ and $\{\mathbf{e}_k\}_{k=0}^M$ in the coordinates $\{\mathbf{u}_k\}_{k=0}^M$ and $\{\mathbf{e}_k\}_{k=0}^M$ by

$$\mathbf{\Phi}_k = \alpha_k \mathbf{u}_k + \beta_k \mathbf{s}_k \quad (10)$$

and

$$\mathbf{e}_k = \eta_k \mathbf{u}_k + \zeta_k \mathbf{s}_k. \quad (11)$$

The expanding and contracting directions follow the linearized maps,

$$\mathbf{u}_{k+1} = \mathbf{L}_k \mathbf{u}_k, \quad (12)$$

and

$$\mathbf{s}_{k+1} = \mathbf{L}_k \mathbf{s}_k. \quad (13)$$

For a random $|\mathbf{u}_0| = 1$, equation (12) gives \mathbf{u}_k aligned with unstable direction at \mathbf{p}_k after just a few iterations. Starting with a random \mathbf{s}_M and iterating (13) backwards gives \mathbf{s}_k aligned with the stable direction at \mathbf{p}_k after a few iterations. Substitute (10) and (11) into (9) to get,

$$\alpha_{k+1} \mathbf{u}_{k+1} + \beta_{k+1} \mathbf{s}_{k+1} = \mathbf{L}_k (\alpha_k \mathbf{u}_k + \beta_k \mathbf{s}_k) + (\eta_{k+1} \mathbf{u}_{k+1} + \zeta_{k+1} \mathbf{s}_{k+1}). \quad (14)$$

Substituting (12) and (13) into (14) yields recursive relationships for $\{\alpha_k\}_{k=0}^N$ and $\{\beta_k\}_{k=0}^N$ where,

$$\begin{aligned} \alpha_{k+1} &= |\mathbf{L}_k \mathbf{u}_k| \alpha_k - \eta_{k+1}, \\ \beta_{k+1} &= |\mathbf{L}_k \mathbf{s}_k| \beta_k - \zeta_{k+1}. \end{aligned} \quad (15)$$

Equations (15) are made computationally stable by calculating the coefficients α_k starting with α_M and iterating backwards and the coefficients β_k are calculated by choosing an initial β_0 and iterating forwards. The choice of α_M and β_0 are arbitrary and are taken to be $\alpha_M = \beta_0 = 0$. Thus the sequence of correction coefficients are given by

$$\begin{aligned} \alpha_M &= 0, & \alpha_k &= (\alpha_{k+1} + \eta_{k+1}) / |\mathbf{L}_k \mathbf{u}_k|, \\ \beta_0 &= 0, & \beta_k &= |\mathbf{L}_k \mathbf{s}_k| \beta_k - \zeta_{k+1}, \end{aligned} \quad (16)$$

where the values of η_k and ζ_k can be determined directly from (5) and (11).

Once $\{\hat{\mathbf{p}}_k\}_{k=0}^M$ has been found, the refinement procedure can be iterated. Generally, the number of significant digits doubles on each iteration of the process. However, cases have

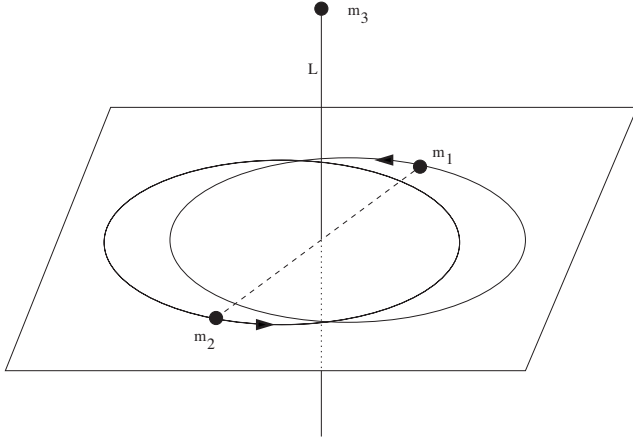


Figure 1. The Sitnikov Problem

been found where the convergence is much slower or does not converge.

The convergence of the refinement procedure does not in itself show the existence of a shadow-orbit. Grebogi et al. (1990) provide a containment procedure in two dimensions which rigorously proves the existence of a shadow-orbit. The containment technique was later extended to three dimensional systems by Hayes (2001). A more practical approach for higher dimensional systems was developed by Sauer and Yorke (1991). They showed that for a given pseudo-orbit, if the refinement procedure converges - to machine precision - and certain quantities of a theorem remain bounded, then the pseudo-orbit has a shadow-orbit.

It has been found (Quinlan and Tremaine 1992; Hayes 2003), that one can tell from the convergence of the refinement procedure alone whether a given pseudo-orbit can be shadowed. So, if iterations of the refinement procedure converge to a new orbit where the one-step errors are the size of machine precision, then it is inferred that a shadow-orbit exists for the given pseudo-orbit. The new orbit found by the refinement procedure is called a **numerical shadow**.

3 THE SITNIKOV PROBLEM

In this study of shadowing for the 3-body problem, a special configuration of the restricted 3-body problem known as the Sitnikov problem will be considered. The Sitnikov problem is the problem of the motion of a mass-less particle, m_3 , on the axis of symmetry of an equal-mass binary (Figure 1). Following Moser (1973), units are chosen such that the gravitational constant $G = 1$ and the total mass $M = 1$. Under these conditions, the equation of motion for m_3 is given by

$$\ddot{z} = -\frac{z}{\sqrt{z^2 + r^2}^3}, \quad (17)$$

where z is the position of m_3 and r the distance from the centre of mass to one of the binary masses. The distance r can be approximated to first order in the eccentricity, e , by

$$r \approx \frac{1}{2}(1 - e \cos t), \quad (18)$$

and the specific energy of m_3 can be defined by

$$E = \frac{1}{2}|\dot{z}|^2 - \frac{1}{\sqrt{r^2 + z^2}}. \quad (19)$$

Taking the plane of motion of the binary ($z = 0$) as a Surface Of Section (SOS), consider a map, $\phi : (v_0, t_0) \rightarrow (v_1, t_1)$, which takes m_3 from one crossing of the SOS to the next. If m_3 is on the SOS at time t_0 , ϕ is a map which brings $v_0 = \dot{z}(t_0)$ to time $t_1 > t_0$ where $v_1 = \dot{z}(t_1)$ and $z(t_1) = 0$. The map ϕ has an open domain D_0 in which every point returns to the SOS. As time enters into the problem with period 2π , D_0 can be considered in polar co-ordinates where the radial variable is v and the angular variable is given by t . Alternatively, the domain D_0 can be considered on the surface of a cylinder where the initial position on the cylinder is defined by t_0 and E_0 . Figure 2 (a) shows the domain for ϕ in cylindrical coordinates. The colour of each point represents the number of periods of the binary before escape happens. The green regions represent islands of quasi-periodic motion. In Figure 3 an example of a quasi-periodic orbit which visits the islands of stability in the vicinity of a period 7 orbit is provided.

3.1 An approximate Poincaré map

Urminsky and Heggge (2009) demonstrated that the Poincaré map ϕ with (18) can be approximated by a symplectic map $\varphi : (t_0, E_0) \rightarrow (t_1, E_1)$ where

$$\begin{aligned} E_{1/2} &= E_0 + a \cos(t_0) + b \sin(t_0), \\ t_{1/1} &= t_0 + 2C(-E_{1/2})^{-3/2}, \\ t_1 &= t_{1/2} + 2C(-E_{1/2})^{-3/2}, \\ E_1 &= E_{1/2} - a \cos(t_1) + b \sin(t_1), \end{aligned} \quad (20)$$

and a , b and C are constants. The quantities $t_{1/2}$ and $E_{1/2}$ are approximations of the time and energy values of m_3 at a local maximum distance from the SOS. It is clear (Figure 2 (a)) that the change in energy of m_3 from one crossing to the next is periodic in time and the trigonometric terms in (20) can be thought of as the lowest order in a Fourier approximation to this change. The change in time is obtained by approximating the motion of m_3 as Keplerian. The constants a and b are proportional to the eccentricity of the binary whose values can be shown to be,

$$\begin{aligned} a &\approx 0.149e \\ b &\approx 0.5075e \end{aligned} \quad (21)$$

and the constant $C = \pi/(2\sqrt{2})$.

3.2 Escape and Capture

Through interactions with the binary as it crosses the SOS, m_3 can gain sufficient energy such that it leaves the SOS and does not return. It can be shown that for some positive time t^* and positive $\nu = (1 - e)/2$, if

$$\frac{1}{2}\dot{z}(t^*)^2 - \frac{1}{z(t^*)^2 + \nu} > 0, \quad (22)$$

then $|z(t)| \rightarrow 0$ as $t \rightarrow \infty$. Setting $z = 0$ in (22) gives a lower bound on the velocity of orbits which escape on the SOS. The solid black region at the top of Figure 2 (a) demonstrates how this condition over estimates the escape boundary. All energy and time values in this region do not return to the SOS.

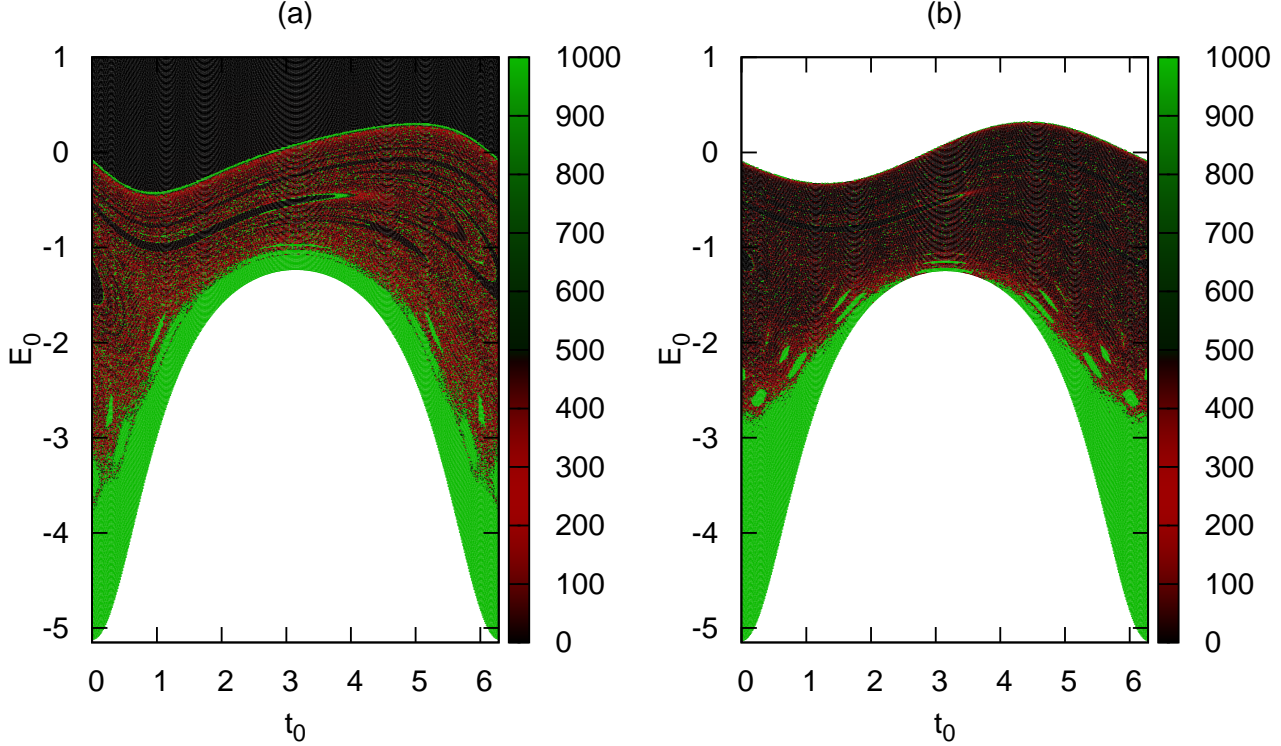


Figure 2. (a) Domain in (t_0, E_0) -space for the map ϕ where $e = 0.61$. Each point represents an initial condition and the associated colour represents the number of periods of the binary before escape. The green regions towards the bottom of the graph represent quasi-periodic orbits which remain bound for all time. The solid black region at the top of the image are initial conditions outside of the domain of ϕ . The escape criterion used is effective in determining escape but crude in approximating the escape boundary on the SOS. (b) Domain in (t_0, E_0) -space for the map φ where $e = 0.61$. The colour associated with each initial condition represents the number of periods of the binary before escape. In (b), the number of periods of the binary is determined by $t_M/2\pi$ where M is the number of iterations of the map. The green regions represent quasi-periodic orbits which do not escape.

The map, φ , provides an accurate way of determining escape and capture. From equation (20) it is found that the mapping φ is defined in a region,

$$E_0 < -a \cos(t_0) - b \sin(t_0) := \partial\mathcal{D}_0, \quad (23)$$

for

$$t_0 \in [0, 2\pi] \quad (24)$$

as time enters into the mapping with period 2π . The curve $\partial\mathcal{D}_0$ is the escape boundary. Time and energy values above $\partial\mathcal{D}_0$ are said to have escaped. The domain, \mathcal{D}_0 , can be defined by (23) and (24). Initial conditions in \mathcal{D}_0 are mapped into the region, \mathcal{D}_1 , defined by

$$E < -a \cos(t) + b \sin(t) := \partial\mathcal{D}_1, \quad (25)$$

for $t \in [0, 2\pi]$. Figure 4 shows how the boundaries $\partial\mathcal{D}_0$ and $\partial\mathcal{D}_1$ intersect. Orbits are mapped from the region under the curve $\partial\mathcal{D}_0$ to the region under the curve $\partial\mathcal{D}_1$. The region $\mathcal{B}_0 = \mathcal{D}_0 \setminus \mathcal{D}_1$ represents energy and time values for which orbits are captured. In the context of the differential equation, these are orbits which come from infinity and get captured

by the binary. Similarly, the initial conditions in the region $\mathcal{B}_1 = \mathcal{D}_1 \setminus \mathcal{D}_0$ are energy and time values for which φ is undefined. Again, in the context of the differential equation, the region \mathcal{B}_1 represents orbits which escape from the system. Finally, note that initial conditions for the differential equation are such that $\dot{z} > 0$ and $z = 0$ on the SOS. So from (19), the initial energy can be bounded from below by,

$$E > -1/|r(t_0)|, \quad (26)$$

for $t_0 \in [0, 2\pi]$.

Initial conditions are chosen in \mathcal{D}_0 with (26) for $e = 0.61$ and plotted in Figure 2 (b). The colour of each point represents the number of periods of the binary determined by $t_M/2\pi$ where M is the number of iterations of the map φ . The green regions represent stable motion whose orbits remain bounded. As energy increases orbits become unstable and escape from the system. Notice the similarities between Figure 2 (a) and 2 (b). Both domains have islands representing stable orbits as well as large regions representing unstable orbits. In Figure 5 an example of a quasi-periodic orbit near a period 7 orbit is provided. In addition to the

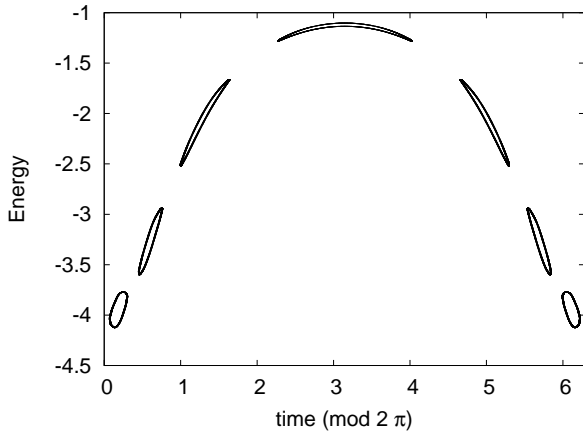


Figure 3. An example of a quasi-periodic orbit near a period 7 orbit for equation (17) on the SOS $z = 0$. Initial conditions are $\dot{z}(0) = 1.3$, $z(0) = 0.0$, $e = 0.61$ and the phase of the binary is .45 radians from pericentre.

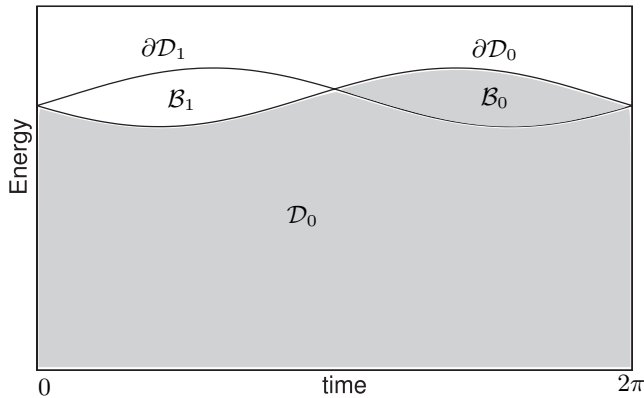


Figure 4. The curve ∂D_0 represents a lower bound of energy and time values for which φ is undefined. Similarly, the curve ∂D_1 represents a lower bound of energy and time values for which the inverse map φ^{-1} is undefined. The shaded region is the domain D_0 for the map φ . The two regions labeled B_0 and B_1 bounded by the curves ∂D_0 and ∂D_1 are the capture and escape regions respectively.

similarities between Figure 2 (a) and (b), Urminsky (2009) demonstrates that the map φ satisfies Lemmas similar to Lemmas 1-5 in Moser (1973) (pages 87-91) and that φ , like ϕ , possesses a hyperbolic invariant set on which φ is topologically equivalent to the shift map.

4 RESULTS

The map φ provides a simple way of studying shadowing for orbits like those of the Sitnikov problem. The approximate map is used to avoid integrating between successive crossings of the SOS thus obtaining a tremendous speed up in calculations. In addition, the one step error can more easily be controlled. At each time step uniformly distributed noise $|\delta_k| \leq \delta$ is added to generate the pseudo-orbit. The refinement procedure is then used to reduce the noise level to machine precision. Since φ is a 2-dimensional mapping,

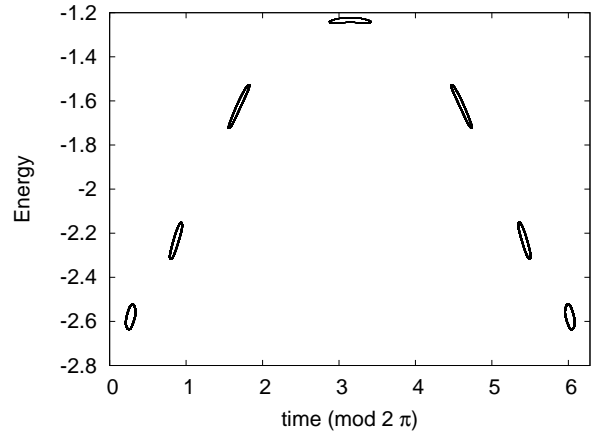


Figure 5. An example of a quasi-periodic orbit near a period 7 orbit for the map φ . Initial conditions are $t_0 = 6.01822$ and $E_0 = -2.5297$ for $e = 0.61$.

the refinement procedure can be directly applied as shown in section 2.1.

4.1 Long lived orbits

Using the containment and refinement procedure, Grebogi et al. (1990) successfully demonstrated the existence of shadows for pseudo-orbits of length 10^7 or more. To test the algorithm the refinement procedure is applied to long lived orbits of the map φ . As seen in Figure 2 (b), there are regions of stable motion where orbits remain bounded forever. The refinement procedure is applied to these orbits and it is found that most can be shadowed for many iterations. Some of these are shown in Figure 9.

As shown by Dvorak et al. (1998) for the Sitnikov problem, the map φ has ‘sticky’ regions where orbits can be trapped for long periods of time before escape. In Figure 6 an example of a sticky orbit trapped in the vicinity of islands of stable quasi-periodic orbits is shown. The inset plot in Figure 6 is a magnification of the orbit near one of the islands. By sampling the phase space around the islands of stable motion, one can find many sticky orbits which survive for long periods of time. In Figure 7 the shadow distance is plotted against the number of iterations of the map for several sticky orbits where $e = 0.61$. It is shown that as the number of iterations increases, the distance of the numerical shadow from the pseudo-orbit increases proportionally to the number of iterations.

4.2 Shadowing capture orbits

Consider uniformly distributed initial values in B_0 (Figure 4) for $e = 0.25$. Initial values are iterated forward for a maximum of 100000 iterations up to the penultimate iteration before escaping. For each orbit, the number of iterations, M , the orbit was ‘shadow-able’ for as well as the shadow-distance are recorded. The orbits are binned into bins of length one iteration and averaged over the bin. The results are plotted in Figure 8 where the dots represent the average shadow-distance at each iteration of the map. Note that as

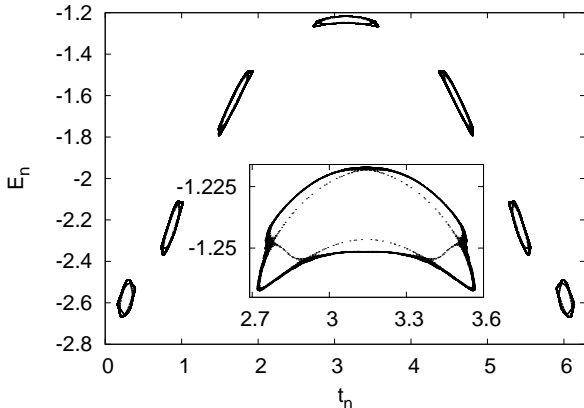


Figure 6. An example of a ‘sticky’ orbit which remains close to islands of stable orbits for the map φ for 500,000 iterations. The inset box is a magnification of the upper most island of stability.

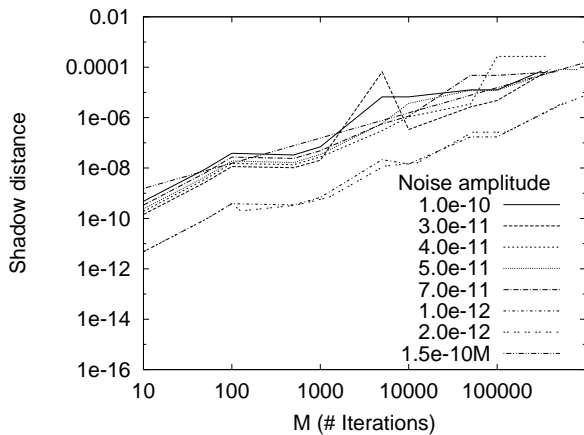


Figure 7. Number of iterations versus shadow distance ϵ .

M increases, there is increasing variability on the distribution of average shadow distances. The data can be fit with the curve $7 \times 10^9 M$ which is similar to the results in Figure 7 where the shadow distance is proportional to the orbit length.

5 WHERE DOES SHADOWING FAIL?

Numerical shadows have been found using the refinement procedure for orbits whose length exceeds 10^5 iterations for the map φ . However, what happens when numerical shadows are not found? What causes the refinement procedure to fail? First, it should be noted that the failure of the refinement algorithm to converge to a numerical shadow does not imply that there is not a shadow-orbit for a given pseudo-orbit. A shadow may still exist but the refinement procedure was not able to converge towards it. Quinlan and Tremaine (1992) and Hayes (2003) found that shadowing breaks down during close encounters between particles. This is due to the stretching of the velocity subspace during a close encounter. In the Sitnikov problem, m_3 interacts with the binary on the SOS and the distance separating m_3 with the binary

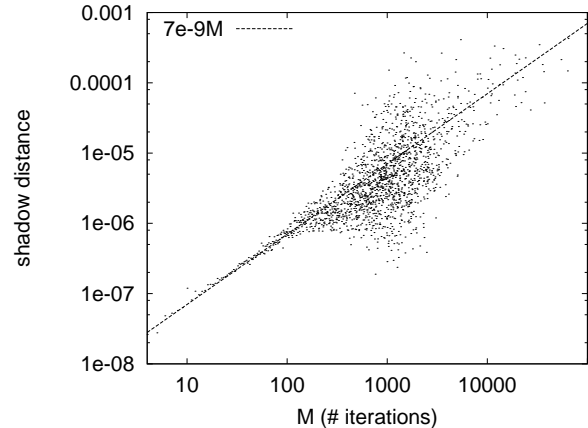


Figure 8. Each point is average shadowing distance for the associate shadow length M for 10^5 initial conditions in \mathcal{D}_0 where $e = 0.25$.

masses is bounded from below (and above) on the SOS. In contrast to the problems discussed in the above mentioned studies arbitrarily close encounters do not occur in the Sitnikov problem. However, escape and capture occur during close encounters with the binary as m_3 crosses the SOS. Near the escape and capture boundaries slight changes in the energy of m_3 as it crosses the SOS can lead to significant changes in the duration of successive crossings of the SOS. The map provides a simple way of sampling the phase space on the SOS to find regions where shadowing is more likely to fail.

Figure 9 shows shadowing results of 10^6 initial conditions. The colour of each point represents either success, yellow, or failure, black, of the refinement procedure. Note that only orbits which survived more than three iterations of the map are considered. This is because the choice of \mathbf{u}_0 and \mathbf{s}_M would influence the results for short lived orbits as (12) and (13) may not have had enough time to align \mathbf{u}_k and \mathbf{s}_k in the proper directions. From Figure 9 it can be seen that the refinement procedure tends to fail near the escape boundary $\partial\mathcal{D}_0$. Note also that the refinement procedure fails near the boundaries of regions containing orbits which escape after three or less iterations.

The reason the refinement procedure fails in these regions is that there is a stretching of subspace as orbits near the boundary $\partial\mathcal{D}_0$. At a given iteration k , the distance from boundary, $\partial\mathcal{D}_0$, is given by,

$$d = |E_k + a \cos(t_k) + b \sin(t_k)|. \quad (27)$$

From the Jacobian of (20) it can be shown that

$$|\mathbf{L}\mathbf{u}_k| \sim d^{-5/2}. \quad (28)$$

Thus, as $d \rightarrow 0$, the correction coefficients α and β go to 0 and ∞ respectively making it more difficult for the refinement procedure to converge.

Figure 10 shows the density of successfully shadowed orbits based on the closest approach to the boundary $\partial\mathcal{D}_0$ for increasing eccentricity values. For each shown eccentricity value, we select 100,000 uniformly distributed initial conditions in the region defined by $t_0 \in (\pi, 2\pi)$ and $E_0 \in (\partial\mathcal{D}_0 + 2b \sin(t_0), \partial\mathcal{D}_0)$. These boundaries describe a band of initial conditions bounded above by the escape

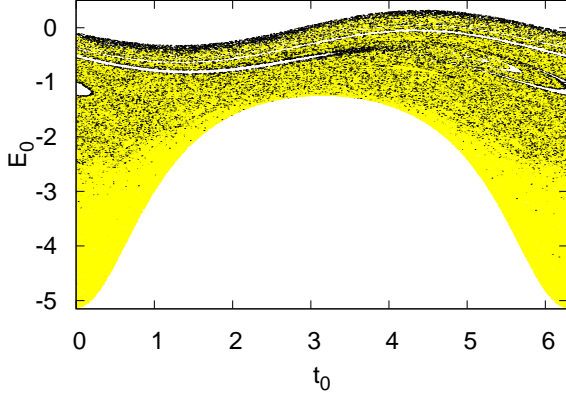


Figure 9. The figure shows one million initial conditions for the map φ where $e = 0.61$. The map φ was applied to each initial condition 50,000 times or until the resulting orbit escaped. The colour associated with each point represents the successful application of the refinement algorithm. Black represents initial conditions where the refinement procedure failed to converge. Yellow represents the successful application of the refinement procedure. Only orbits which were longer than three iterations of φ are considered.

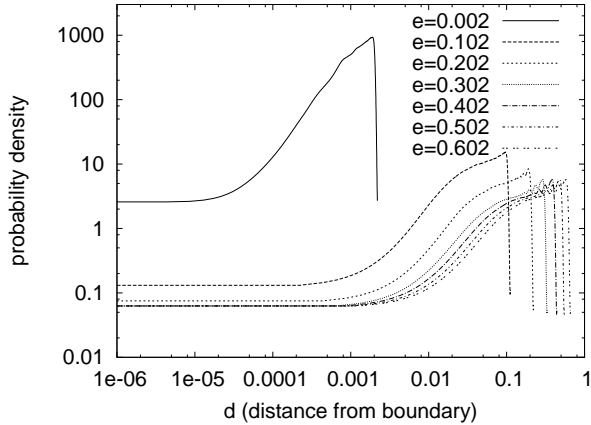


Figure 10. Probability density of close approaches to the escape boundary for shadowable orbits.

boundary. This band also encompasses the capture region \mathcal{B}_0 . The drop in the density to the right of each curve occurs at the distance between the lower boundary curve and the escape boundary. Note that the density drops off as initial conditions approach the escape boundary. Data was fitted using a variable bandwidth kernel density function.

5.1 Probability of capture

It was found above that as orbits approach the escape boundary the likelihood of an orbit being shadowed decreases. This has an impact on the shadowability of orbits in the capture region \mathcal{B}_0 . The capture region area is directly proportional to the eccentricity of the binary. As $e \rightarrow 0$, the initial conditions in \mathcal{B}_0 become pushed up against the

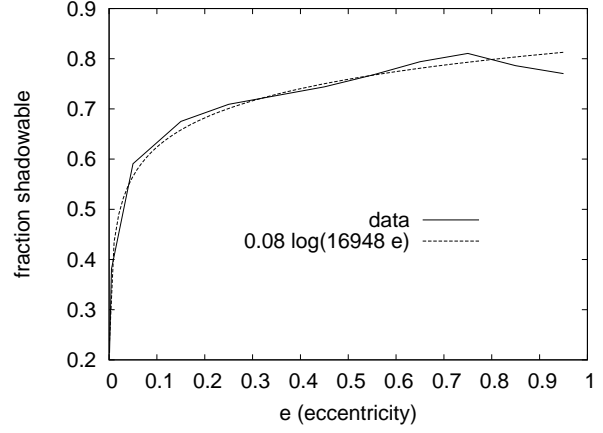


Figure 11. Fraction of capture orbits shadowable using the refinement procedure for increasing eccentricities of the binary.

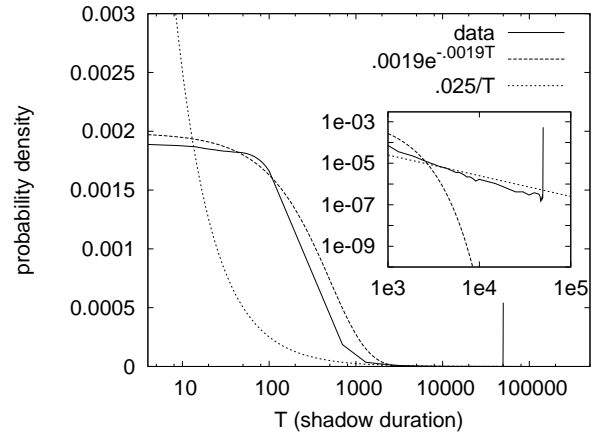


Figure 12. Probability density of shadow durations for the map φ where $e=0.61$. The amplitude of the one step noise was set at 10^{-9} . For shadow durations $T < 5000$ the density can be approximated by an exponential distribution. For larger T the density is inversely proportional to T .

boundary $\partial\mathcal{D}_0$. It is expected then that for small eccentricities, orbits would be less likely to be shadowable.

To test this hypothesis, 10^5 uniformly distributed initial conditions are selected in \mathcal{B}_0 and iterated forwards until each orbit escapes. This is performed for a variety of eccentricity values and the fraction of shadowable orbits in each case is determined. The results are shown in Figure 11. The fraction of shadowable orbits increases as the eccentricity of the binary increases. This is because the area of the capture region increases proportionally to e . As the area increases, initial conditions can be selected at a much further distance from the escape boundary making them more likely shadowable.

5.2 Failure as a stochastic process

The failure of the refinement procedure can happen at any point along the orbit and not necessarily at a close approach to the escape boundary. The shadow duration is defined as the number of iterations for which a given orbit can be shad-

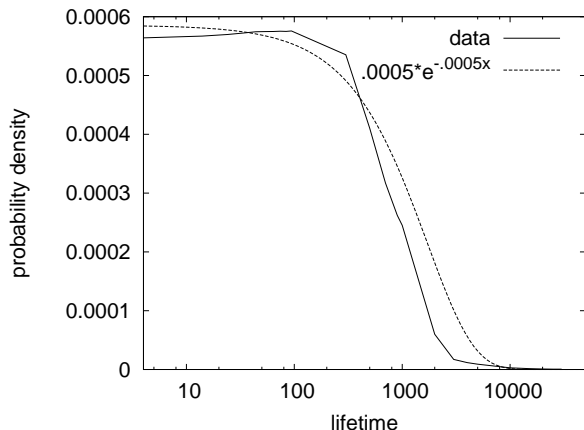


Figure 13. Probability density for the lifetime, $\sum_{k=0}^T t_k$, for the map φ where $e=0.61$. The amplitude of the noise is 10^{-9} . It was found that the distribution best fit an exponential distribution.

owed. For an orbit $\{(t_i, E_i)\}_{i=0}^M$ the shadow duration, T , can take on positive integer values $T < M$.

Consider the initial conditions for $e = 0.61$ shown in Figure 9. For each resulting orbit, it is determined how long the orbit is shadow-able. Figure 12 provides some information on the distribution of shadow lengths. Initial conditions are chosen in \mathcal{D}_0 and iterated forwards in time using (20). Each orbit is iterated for 50,000 iterations or until the solution escapes. The solid line in Figure 12 represents the density of the numerical experiments. The spike at 50,000 iterations is mostly due to quasi-periodic orbits which remain bounded for all time. As shown in Figure 12, the density can be approximated, for small iterations, by an exponential density function given by $\xi \exp(-\xi x)$ for $\xi = 0.0019$. The inset graph is a magnification of the density for $1000 < M < 50,000$. In this range, the density function is better represented by the function $.025/M$.

The map approximates the time between crossings of the SOS by considering the motion of m_3 to be Keplerian. Instead of considering the distribution of the shadow duration in terms of the number of iterations of φ we can instead consider the distribution of shadow times, t_M where M is the number of iterations of the orbits for which it was shadow-able. The solid line in Figure 13 represents the probability density of shadow time for the numerical experiments. Again, the data can best be approximated by the exponential density function for $\xi = .0005$. The results found here are in agreement, for small shadow durations, with previous results by Hayes (2003) which showed that shadow durations for larger N -body systems have an exponential distribution and can be thought of as a Poisson process.

6 CONCLUSIONS

The above results confirm, for short lived orbits, previous investigations (Hayes 2003) that showed numerical shadow durations, M , for gravitating systems follow a Poisson process with a exponential density function. The result found in this study suggests for longer lived orbits, the density function is better approximated by a function proportional to $1/M$. This may be because the population of longer lived

orbits tends to be dominated by stable orbits, however this has not been investigated.

In section 5, areas of phase-space where the refinement procedure is more likely to fail are characterized. These areas are near escape boundaries where there is sufficient stretching of phase-space to cause the refinement procedure to fail to converge to a less noisy orbit. Interestingly this seems to be due to the growth of the variational equations over one time step. This does not rule out the failure of the the refinement procedure by the accumulative effect of the growth of the variational equation associated with large Lyapunov exponents as discussed by Zhu and Hayes (2009).

In Figure 11 it is demonstrated that as the volume of phase-space representing capture orbits decreases, it becomes increasingly difficult to shadow capture orbits. This is a result of the distribution of failures of the refinement procedure seen in Figure 10. As the volume of phase-space associated with capture decreases, capture orbits get pushed up against the boundary $\partial\mathcal{D}_0$ where the one-step growth of the variational equations causes the refinement procedure to fail.

Finally, it was found that the shadow distance for an orbit is proportional to the number of iterations of the map (Figures 7 and 8). It was noticed that if in addition to t_1 and E_1 , orbits were required to be shadow-able at the half steps $t_{1/2}$ and $E_{1/2}$, then initially shadow-able orbits continued to be shadow-able. When shadowing at the half step was required, the shadow distance typically increased by about a factor of two.

The Sitnikov problem discussed in this study provides a straight forward way of characterizing a domain of initial conditions as well as regions of stable and unstable motion. Work in progress considers slight changes to the Sitnikov problem in order to study shadowing of unstable orbits. For example, Soulis et al. (2007) consider slight perturbations to the mass and position (away from the z -axis) of m_3 and delineate regions of stable and unstable motion. It would be expected that, like the results found in this study, shadowing with the refinement procedure breaks down near boundaries of escape for unstable orbits. In fact, the break down of the refinement procedure near escape boundaries would be expected for general 3-body configurations. As solutions approach parabolic escape boundaries, an orbit can undergo increasingly long ejections from the left-over binary system. Small changes in the energy of an orbit in this region can cause significant changes in the time of return for the orbit. If the refinement procedure could make changes to the orbits so as to conserve the energy of the ejected body it might improve the success rate of the refinement procedure. Finally, the Sitnikov 4-body problem (Soulis et al. 2008) provides a starting point for examining the relationship between the shadowing distance and the number of bodies. Extra bodies can be added in circular orbits about the center of mass. Hayes (2003) demonstrates that as the number of moving bodies in a fixed potential increases the shadow durations decrease. It would be of interest to determine if a similar relationship holds for the Sitnikov N -body problem.

It should be stressed again that the failure of the refinement procedure does not necessarily mean that a shadow does not exist for a given pseudo-orbit. It may very well be that shadows do exist for orbits in regions where the refinement procedure fails. We are encouraged that this may be

the case. Both the Sitnikov problem and the approximate Poincaré map possess a hyperbolic invariant set, Λ , near the escape boundaries (see Moser (1973) and Urmitsky (2009) respectively). Despite the fact that Λ is near the boundary $\partial\mathcal{D}_0$, the shadowing theorems by Anosov (1967) and Bowen (1972) guarantee that any pseudo-orbit on Λ has an associated shadow-orbit. This demonstrates that being in the vicinity on the escape boundary does not necessarily rule out the existence of shadow-orbits.

ACKNOWLEDGMENTS

DU was supported by the National Aeronautics and Space Administration through grant NNX-07AH15G. The author would like to thank D. Heggie, D. Merritt and D. Dicken for their helpful suggestions. In addition, the author would like to thank the anonymous referee for his/her careful reading of the manuscript and useful suggestions.

REFERENCES

- Anosov D.V, 1967, Trudy Mat. Inst. Steklov, 90, 209
 Bowen R., 1972, Amer. J. Math., 94, 1
 Chow S., Lin X., Palmer K.J., 1989, Differential equations, Lecture Notes in Pure and Appl. Math., 118, Dekker, New York, 127
 Chow S., Palmer K.J., 1991, J. Dynam. Differential Equations, 3, 3, 361
 Chow S., Van Vleck E., 1994, SIAM J. Sci. Comput., 15, 4, 959
 Coomes B.A., Koçak H., Palmer K.J., 1994, J. Comput. Appl. Math., 52, 35
 Coomes B.A., Koçak H., Palmer K.J., 1995, Z. Angew. Math. Phys., 46, 1, 85
 Dejonghe H., Hut P., 1986, in Hut P., McMillan S., eds, The Use of Supercomputers in Stellar Dynamics, Lecture Notes in Physics, 246, Springer, Berlin, 212
 Dvorak R., Contopoulos G., Efthymiopoulos C., 1998, Planet. Space Sci., 46, 1567
 Goodman J., Heggie D.C., Hut P., 1993, ApJ, 415, 213
 Grebogi C., Hammel S.M., Yorke J.A., Sauer T., 1990, Phys. Rev. Lett., 65, 1527
 Hayes W.B., 2001, Ph.D. thesis, University of Toronto, Toronto
 Hayes W.B., 2003, Phys. Rev. Lett., 90, 5, 054104
 Heggie D.C., 1991, in Roy A.E., ed., Predictability, Stability and Chaos in N -Body Dynamical Systems, Plenum Press, New York, 47
 Hemsendorf M., Merritt D., 2002, Apj, 580, 606
 Kandrup H.E., Smith H., 1991, ApJ, 374, 255
 Kato K., 1991, Mem. Fac. Sci. Kochi Univ. Ser. A Math., 21, 43
 Nadzieja T., 1991, Arch. Math. (Brno), 27A, 65
 Lecar M., 1968, Bull. Astron., 91, 3, 213
 Miller R.H., 1964, ApJ, 140, 250
 Moser J., 1973, Stable and Random Motions in Dynamical Systems, Princeton U. Press, Princeton
 Quinlan G.D., Tremaine S., 1992, MNRAS, 259, 505
 Sauer T., Yorke J.A., 1991, Nonlinearity, 4, 961
 Soulis P., Bountis T., Dvorak R., 2007, Celest. Mech. Dyn. Astron., 99, 129
 Soulis P.S., Papadakis K.E., Bountis T., 2008, Celest. Mech. Dyn. Astron., 100, 251
 Standish E.M., 1968, Ph.D. thesis, Yale University, New Haven
 Urmitsky D.J., Heggie D.C., 2009, MNRAS, 392, 1051
 Urmitsky D.J., 2009, Ph.D. thesis, University of Edinburgh, Edinburgh
 Van Vleck E., 1995, SIAM J. Sci. Comput., 16, 5, 1177
 Zhu Y.-K., Hayes W.B., 2009, AAS/Division of Dynamical Astronomy Meeting, 40, 11